Deformation analysis of the seawall in Qiantang estuary with multi-temporal InSAR

ZHANG Yunjun[1,3], WAN Zi[2], XIE Chou[1], SHAO Yun[1], YUAN Minghuan[1,3], CHEN Wu[2], WANG Xin[2]

1. *Institute of Remote Sensing and Digital Earth (RADI), Chinese Academy of Sciences, Beijing* 100101, *China*;
2. *Zhejiang Institute of Hydraulics and Estuary, Hangzhou* 310020, *China*;
3. *University of Chinese Academy of Sciences, Beijing* 100049, *China*

Abstract: Deformation monitoring is essential to the safe operation of seawalls. This paper reports the Interferometric Synthetic Aperture Radar (InSAR) measurement results derived from 31 Envisat ASAR images acquired over Hang zhou from 2006 to 2010, with special focus on the seawall in the Qiantang Estuary. Multi-temporal InSAR (MTInSAR) was used to extract deformation information from both Persistent Scatterers (PSs) and Distributed Scatterers (DSs), which provide dense measurement of the deformation of the seawall. Compared with the leveling measurement at 28 points, the mean error derived by InSAR is 0.436 mm, with the largest error of 5.016 mm, which confirms the millimeter-level precision and accuracy of the InSAR technique. A time series analysis was conducted based on these two datasets, and results showed that the subsidence of seawalls was spatially continuous and had a local negative unimodal pattern with distance. A linear tendency with minor local fluctuation was also observed in the time domain during a period of nearly seven years.

Key words: MTInSAR, PS, DS, seawalls in Qiantang Estuary, subsidence

CLC number: P228 **Document code**: A

Citation format: **Zhang Y J, Wan Z, Xie C, Shao Y, Yuan M H, Chen W and Wang X. 2015. Deformation analysis of the seawall in Qiantang estuary with multi-temporal InSAR. Journal of Remote Sensing, 19(2): 339-354 [DOI: 10.11834/jrs.20154055]**

1 INTRODUCTION

The Qiantang Estuary is known as the world's largest tidal bore. The seawall (sea dike) along its banks serves as an important defense of the Hang-Jia-Hu and Xiao-Shao-Ning plains against coastal erosion and other damages caused by wave action and storm surges. Along with the Great Wall and Grand Canal, the Qiantang Seawall is one of the three most famous civil engineering projects in ancient China and remains functional to the present day (Jiang & Tao, 2002). Dangers caused by the deformation of the trunk and gate of the seawalls have emerged after many years because of the effect of typhoon storms, tidal bore, and soft foundation (Yue, 2009). Therefore, developing a near-real-time technique of deformation monitoring for the seawall is important.

Conventional leveling is the oldest and still the main technique of deformation measurement for seawalls in China(Yue & Fang, 2012). GPS has become widely used in recent years given the availability of satellite geodesy (Xu, et al., 2004). Based on sparse discrete measurements, these two techniques usually have low data densities and may therefore fail to detect abrupt changes. Conducting a survey across a wide area is impractical because of the long period of time and high cost needed. Numerical modeling and finite element methods have been developed to analyze and predict the subsidence of soft marine clay and to improve current understanding of the deformation process of embankments (Jiang, et al., 2010; Ministry of Water Resources of China, 2009). They apply well in newly built seawalls during the construction period and several years afterward, but lose power as the seawall ages, during which natural subsidence prevails.

Interferometric Synthetic Aperture Radar (InSAR) provides measurement of ground surface displacement with high spatial resolution and acceptable accuracy in a wide coverage at an extremely low cost(Rosen, et al., 2000). In particular, interferometric stacking techniques, such as persistent scatterer InSAR (PSInSAR) (Ferretti, et al., 2001) and small baseline subset algorithm(SBAS)(Berardino, et al., 2002), renders possible the extraction of long-time deformation by processing series of images and reducing the effects of temporal and geometric decor-

Received: 2014-03-17; **Accepted**: 2014-06-25; **Version of record first published**: 2014-07-02

Foundation: Ministry of Water Resources of China Special Funding for nonprofit Industry Research (No. 201201043)

First author biography: ZHANG Yunjun (1989—), male, master, his research interests are algorithm development and application of radar interferometry. E-mail: jiuncheung@gmail.com

Corresponding author biography: WAN Zi (1982—), male, engineer, his main research interest is hydraulic remote sensing application. E-mail: wanzi021@163.com

relation and atmosphere. These techniques have been successfully applied in urban areas, such as New Orleans, Tianjin, and Berlin (Dixon, et al., 2006; Fan, et al., 2008; Gernhardt & Bamler, 2012; Perissin & Wang, 2011; Zhang, 2008). However, the time series deformation analysis of linear infrastructures has not been intensively studied (Di Martire, et al., 2014; Perissin, et al., 2012; Shi, et al., 2014), and even fewer for seawalls (Pei, et al., 2013).

The present study uses multi-temporal InSAR (MTInSAR) to extract both persistent scatterers (PSs) and Distributed Scatterers (DSs) to obtain a dense measurement for time series deformation. The spatial distribution and time series trend of the seawall's deformation are explored with support from leveling data.

2 STUDY AREA AND DATASETS

A rectangular area of 82 km ×40 km (29°59′40″N—30°28′49″N, 119°55′06″E—20°50′13″E) in Hangzhou, the capital of Zhejiang Province in eastern China, was chosen as the test site. It is located at the south-central portion of the Yangtze River Delta. This area covers about 268 km of the standing seawalls, with the Qiantang River flowing from west to east (Fig. 1). The ancient seawalls that have been preserved to the present day were constructed mainly during the Ming and Qing Dynasties. Most of these seawalls have moved inland because of the changes in the coastline, and what was left has been reinforced into a standardized seawall (Chen & Zhou, 1999); as such they are not included in this study.

Fig. 1 Location of the study area and the SAR amplitude image averaged from 31 ASAR images
(Left: The base map is a microsoft bing aerial photo; white rectangles denote the coverage of 31 ASAR images; the white arrow denotes the satellite flight direction; the orange rectangle denotes the coverage of the study area; the red curves denote the leveling routes)

This study utilizes a total of 31 scenes of 20 m (range) × 4 m (azimuth) resolution C-band (wavelength of 5.6 cm) SAR images acquired by Envisat ASAR from January 5, 2006 to January 14, 2010 along the ascending orbit. All of them were imaged at an incidence angle of 22.8° in VV polarization mode. More parameters are presented in Table 1. A total of 12 temporal fourth-order leveling data were also collected from August 2009 to November 2012. They consist of 136 points distributed along the Qiantang Estuary, as shown in Fig. 1. SRTM3 DEM and historical weather data over Hangzhou were also used.

3 MULTI-TEMPORAL INSAR PROCESSING

Hangzhou has a humid subtropical climate with four distinctive seasons and is characterized by plentiful rain and high forest coverage rate. All these contribute to temporal decorrelation and severe atmospheric phase screen. Various environments along hundreds of kilometers of the seawall lead to a sparse and non-uniform distribution of strong point scatterers, thereby rendering the place unsuitable for PSInSAR application. SBAS implements interferograms of small spatial and temporal baselines, which extenuates the decorrelation phenomena, and maybe a better technique than PSInSAR for seawalls' deformation monitoring of the seawall. However, multilooking reduces spatial resolution, which is a critical parameter, considering the typical 17.5 m wide seawall and 20 m resolution of SAR image. The MTInSAR proposed by Hooper (2008) was used to extract both PSs and DSs and to retrieve a dense and uniform point network without resolution loss, thereby utilizing the advantages of PSInSAR and SBAS. The MTInSAR processing flow chart is shown in Fig. 2.

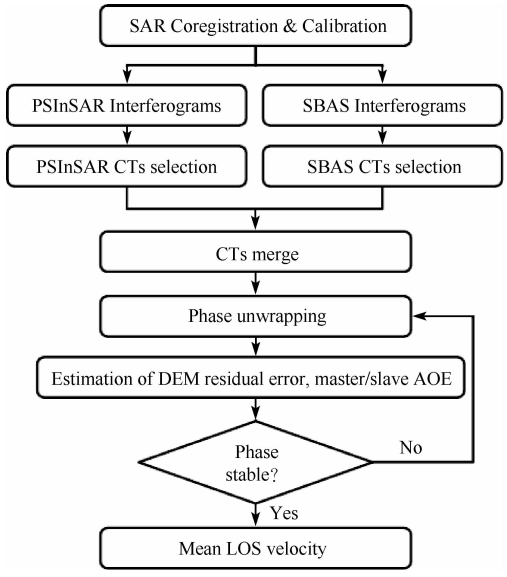

Fig. 2 InSAR processing flow chart

A threshold (0.75) method of coherence ρ was used during the interferometric pair selection of SBAS, which was estimated through a function based on the temporal baseline T and perpendicular spatial line $B_\perp$ (Hooper, 2006):

$$\rho = \left(1 - f\left(\frac{B_\perp}{B_\perp^c}\right)\right) \cdot \left(1 - f\left(\frac{T}{T^c}\right)\right) \quad (1)$$

$$f(x) = \begin{cases} |x|, & |x| \leqslant 1 \\ 1, & |x| > 1 \end{cases} \quad (2)$$

where $B_\perp^c$ indicates the critical perpendicular spatial baseline for ASAR data, which is 1106 m, and T^c indicates the critical temporal baseline, which is 1500 days in this case. The heavy rainstorms in May 29, 2008 and August 27, 2009 (denoted by the orange diamond-shaped points in Fig. 3) caused strong atmospheric disturbance in seven interferograms, in which the deformation phase was totally drowned. Thus, they were dropped and not included in the post-processing. For a full time range of deformation retrieval, two interferograms (denoted by the arrows in Fig. 3) were added to form a connected network of interferograms. A total of 63 interferograms were selected for SBAS, as shown by the dashed lines in Fig. 3.

A total of 79 differential interferograms (i.e., 30 by PSInSAR, 63 by SBAS, and 14 duplicated) were generated by Delft Object-oriented Radar Interferometric Software (DORIS) using the Shuttle Radar Topography Mission (SRTM) with three arc-seconds (90 m) to remove the topographic phase. Coherent targets (CTs) were selected by the Stanford Method for Persistent Scatterers software with PSInSAR and SBAS methods. Their selection results were merged based on the CTs' positions, and overlapping CTs were abandoned. The Atmospheric and Orbit Error (AOE) of the master and slaves, mean Line-Of-Sight (LOS) deformation velocity, and time series deformation were calculated through the iterative phase unwrapping and estimation of the DEM residual error.

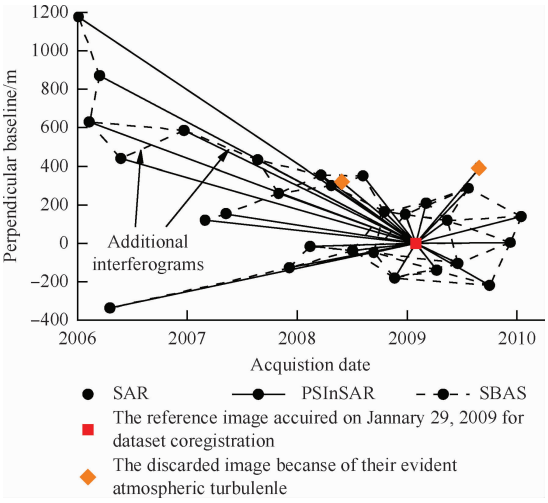

Fig. 3 Interferometric configuration of MTInSAR

Table 1 Basic parameters of Envisat ASAR over Hangzhou

No.	Date	Orbit	$B_\perp$/m	Btemp/d	f_DC diff/Hz
1	2006-01-05	20133	1175.1	−1120	11.32
2	2006-02-09	20634	630.9	−1085	5.51
3	2006-03-16	21135	871.1	−1050	1.15
4	2006-04-20	21636	−336.7	−1015	3.08
5	2006-05-25	22137	439.5	−980	−0.43
6	2006-12-21	25143	585.9	−770	−20.36
7	2007-03-01	26145	120.5	−700	1.21
8	2007-05-10	27147	153.3	−630	7.64
9	2007-08-23	28650	432.0	−525	10.62
10	2007-11-01	29652	260.4	−455	4.59
11	2007-12-06	30153	−126.2	−420	−9.09
12	2008-02-14	31155	−15.5	−350	1.84
13	2008-03-20	31656	355.3	−315	6.85
14	2008-04-24	32157	300.6	−280	5.13
15	2008-05-29	32658	319.5	−245	6.53
16	2008-07-03	33159	−37.8	−210	−2.00
17	2008-08-07	33660	350.8	−175	3.30
18	2008-09-11	34161	−47.6	−140	8.56
19	2008-10-16	34662	165.4	−105	7.04
20	2008-11-20	35163	−179.4	−70	3.05
21	2008-12-25	35664	151.3	−35	6.73
22	2009-01-29	36165	0	0	0.00
23	2009-03-05	36666	209.8	35	5.70
24	2009-04-09	37167	−140.9	70	6.59
25	2009-05-14	37668	118.4	105	8.59
26	2009-06-18	38169	−104.4	140	7.89
27	2009-07-23	38670	285.5	175	−1.73
28	2009-08-27	39171	390.6	210	15.09
29	2009-10-01	39672	−218.2	245	6.58
30	2009-12-10	40674	3.8	315	−2.11
31	2010-01-14	41175	138.8	350	5.57

4 RESULTS AND DISCUSSION

4.1 InSAR Results

The mean LOS deformation velocity over Hangzhou is presented in Fig. 4, where negative values indicate the increase in the distance between the surface and satellite (i.e., the subsidence), whereas the positive values indicate lift up. The averaged point density was 113.6 per square km; the velocity range was [−27.7, 11.4] mm/a; and the corresponding standard deviation (STD) was [0.9, 11.4] mm/a. The maximum deviation was located at the eastern edge and southwest corner of the study area. The major STD was about 1.5 mm/a, which confirmed the stability of InSAR retrieval results.

The detailed results of PSInSAR and MTInSAR on outside section V to IX seawall in Xiaoshan inning (denoted by black rectangle in Fig. 4) are shown in Fig. 5. The MTInSAR method retrieved more CTs on seawalls than the PSInSAR method. Mea-

surement and statistics showed that, on this 9 km seawall, PSInSAR extracted 36 CTs with a corresponding point density of 4 per km, which is similar to the measurement density of leveling (2 to 3.3 per km). By contrast, MTInSAR extracted 99 CTs with a corresponding point density of 11 per km, which is much higher than that of PSInSAR and leveling. These results confirm the superiority of the MTInSAR method on the deformation monitoring of seawalls.

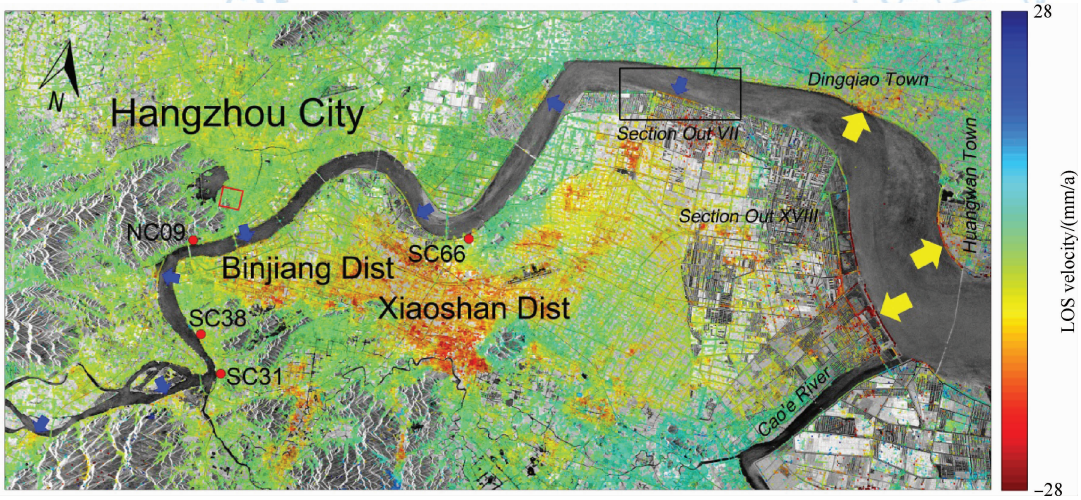

Fig. 4 Mean LOS deformation velocity distribution of Hangzhou during January 2006 to January 2010 (The positive value indicates lift up; the negative value indicates subsidence; the base map is the averaged amplitude of 31 ASAR images; the yellow and blue arrows mark the subsiding seawalls in Hangzhou Bay and Qiantang Estuary respectively; and the red square marks the reference area for deformation)

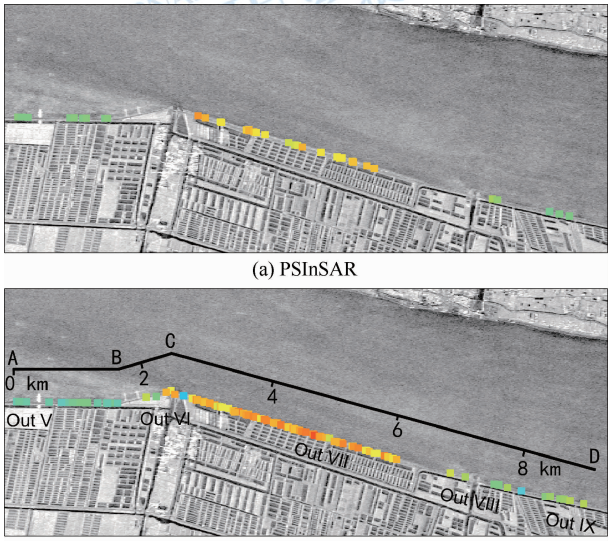

Fig. 5 Distribution of CTs on outside section V to IX in Xiaoshan inning

The overall statistics revealed ten subsiding segments of the seawalls along the Qiantang River during 2006 to 2010: seven in the Qiantang Estuary (denoted by the blue arrows in Fig. 4) and three in Hangzhou Bay (denoted by the yellow arrows in Fig. 4). The latter is larger than the former in terms of both amplitude and spatial range. During this period, the seawalls from outside section Ⅷ to the Cao'e River along the southern bank of Hangzhou Bay, in Huangwan Town and Dingqiao Town along the northern bank of Hangzhou Bay, and from outside section Ⅵ to Ⅷ along the south bank of Qiantang Estuary suffered the most with a mean LOS velocity of over 20 mm/a.

4.2 Comparison with Leveling

Twelve temporal fourth-order leveling data at 136 points along the Qiantang Estuary were collected from August 2009 to November 2012 to assess the accuracy of the InSAR measurement. Its routine is indicated by the red curves in Fig. 1. To minimize the error caused by the position differences of the CTs and leveling points, three principals were set during the corresponding selection of CTs: (1) CTs should be selected around a leveling point within a certain distance (100 m in this case, considering the 20 m resolution of ASAR data). (2) CTs located on and inside the breakwater, where all leveling points are set, should be selected because different parts of the seawall, such as the boulders on the slope protection, the breakwater along with its inside, and the road it is connected to, have different deformation patterns. (3) The data that share the same observation period for the whole time ranges of InSAR (from January 5, 2006 to January 14, 2010) and leveling (from August 2009 to December 2012) should be selected. The mean values of all qualified CTs (transferred from LOS to vertical direction) were compared with their corresponding leveling measurements.

Based on the principles described above, 28 points were selected; July 23, 2009 to December 10, 2009 was used for the time range of InSAR; and August 15, 2009 to November 27, 2009 was used for the time range of leveling. Their comparison is shown in Fig. 6; the two measurements are generally very simi-

lar. The mean subsidence error derived between InSAR and leveling was 0.436 mm with a standard deviation of 1.582, which confirms its millimeter-level precision and accuracy. The largest difference was 5.016 mm at point SC68. This leveling point was located on the road connected to the breakwater, while the corresponding CT was on a manhole cover; thus, the difference in their deformations is reasonable.

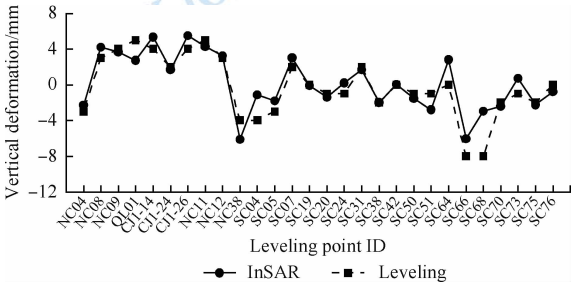

Fig. 6 Comparison of InSAR and leveling

4.3 Spatial distribution

Outside section Ⅴ to Ⅺ seawall in Xiaoshan inning was chosen to analyze the spatial distribution of the deformation of the seawalls (see black rectangle in Fig. 4 for the location and Fig. 5 (b) for the details). This seawall belongs to the northern front of Xiaoshan inning. Outside section Ⅵ to Ⅷ seawall was built in 2002 for 50 years of flood control standard. However, its toe protection was not deep enough to withstand erosion, and many blocks on the slope protection were washed away when the main tides reached the wall or the tidal bore hit the top (Xiaoshan District Agricultural and Water Conservancy Bureau, 2009). It was subsequently strengthened from December 2009 to November 2010 for 100 years of flood control standard (Xu, 2010).

Outside section Ⅴ to Ⅸ seawall can be simplified into three line segments: AB, BC, and CD as shown in Fig. 5(b). The distances of all the CTs from point A along these line segments were calculated and projected in the deformation-distance plane in Fig. 7. The seawall's subsidence was continuous in space and its spatial distribution satisfied a local negative unimodal curve. Among these, outside section Ⅵ to Ⅷ seawall suffered evident subsidence, while outside section Ⅴ and Ⅸ seawall was relatively stable. This deformation trend measured by InSAR was consistent with the actual situation. Finally, time series deformation of the whole study area is presented in Fig. 8.

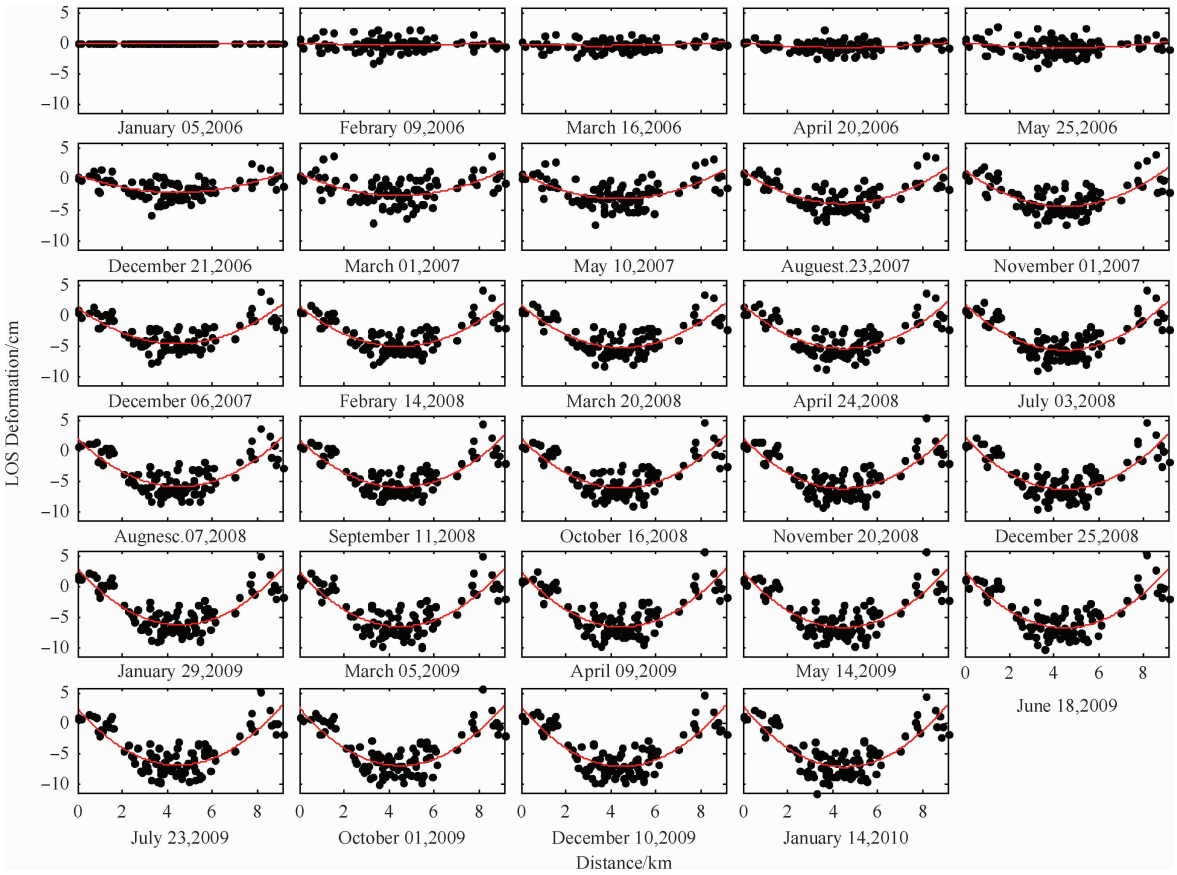

Fig. 7 Time series spatial distribution of seawall's deformation in Outside section Ⅴ to Ⅸ (Deformation is calculated with January 5, 2006 as reference; distance is calculated along the line segments from point A; red curves indicate fitting tendency)

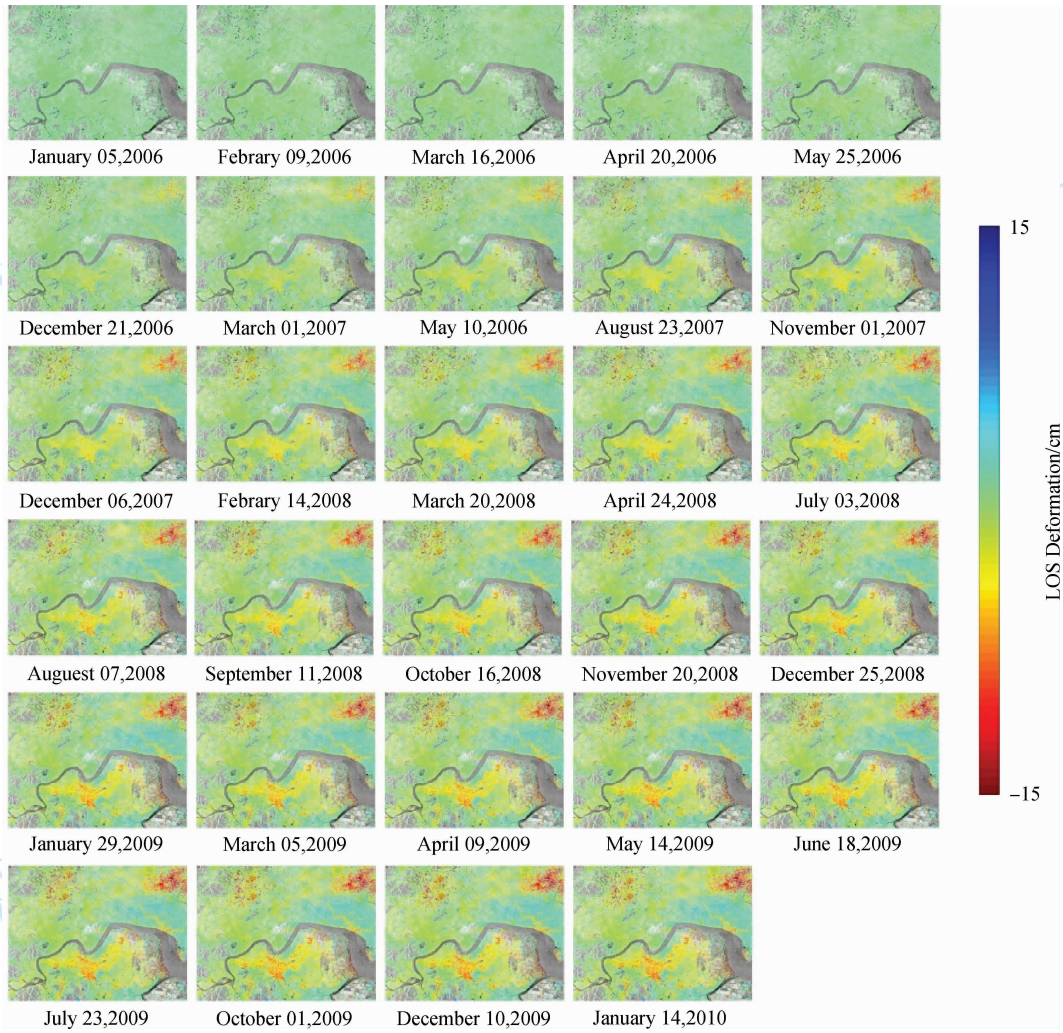

Fig. 8 Time series LOS deformation of Hangzhou area

4.4 Time series trend

The 28 points above were sorted in ascending order and then classified into four categories based on the overall deformation measured by leveling, as displayed in Fig. 9. The majority has a subsidence of 3 cm or less from August 2009 to November 2012.

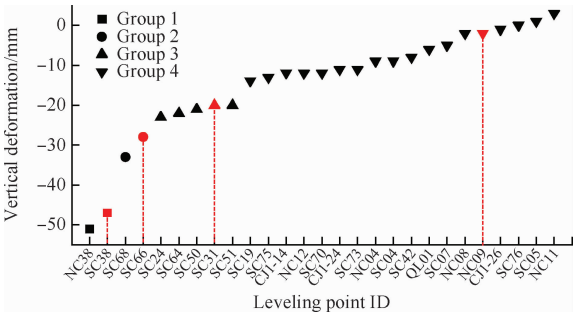

Fig. 9 Overall deformation measured by leveling

A point was selected from each of the four categories for the time series analysis. Their locations are marked by red points in Fig. 4, and their time series deformations are shown in Fig. 10, where InSAR data are represented by solid line with dots on the left of each sub-plot and leveling data are represented by dashed lines with square points on the right. A relatively long time range (seven years from January 2006 to November 2012) of deformation measurement was obtained by combining these two datasets because of the minor temporal overlap of the InSAR and leveling data.

The multi-temporal subsidence of the seawalls, as shown in Fig. 10, exhibits small fluctuations in both InSAR and leveling measurements. However, the seawalls generally showed a linear subsiding tendency during the whole period of time. Linear regression was conducted to assess the linear tendency and estimate the mean subsiding velocities of the seawalls. The results are shown as red lines in Fig. 10. This good fitting reaffirms the consistency of InSAR and leveling measurement. The estimated linear subsiding velocities are listed in Table 2. SC38 point has the largest subsidence velocity of 12.6 mm/a, which has led to an accumulative subsidence of 8.7 cm during the seven years. The NC09 point is the most stable point, with a subsidence velocity of 0.05 mm/a, which is negligible.

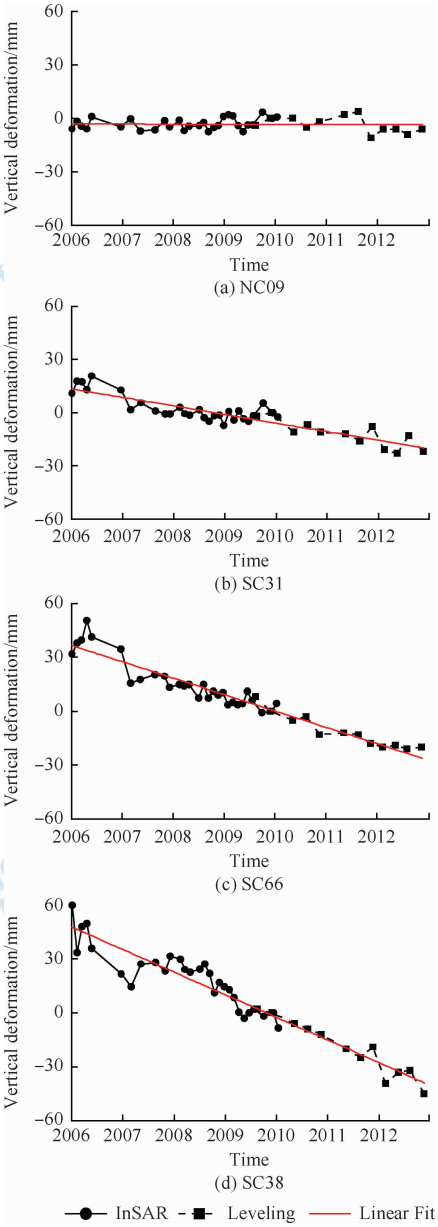

Fig. 10 Time series deformation of four points on the seawall

Table 2 Linear regression estimation of subsidence velocity from 2006 to 2012

Leveling point ID	SC38	SC66	SC31	NC09
Velocity/(mm/a)	−12.6	−9.1	−4.8	−0.05

5 CONCLUSIONS

This paper reported the time series deformation of the Hangzhou area from 2006 to 2010 by processing 31 C-band ASAR data with MTInSAR technique, which extracted both PSs and DSs, thereby providing dense subsidence measurements of the seawall in the Qiantang Estuary. The comparison with leveling data confirmed the precision of InSAR measurement and its feasibility in the deformation monitoring of seawalls. The results show that ten segments are undergoing subsidence, and the situation in Hangzhou Bay is more severe than that in the Qiantang Estuary in terms of amplitude and spatial range. The time series analysis based on InSAR and leveling data show that the deformation of seawalls is continuous. The data also exhibit a local negative unimodal curve in space, while following a linear declining tendency with local fluctuation in the temporal domain.

Future work will be focused on algorithm design to increase the measurement density and exploration of the causes of the deformation of the Qiantang River seawall.

Acknowledgement: Thank ESA for providing the Envisat ASAR data over Hangzhou, the Geospatial Data Cloud of Computer Network Information Center in the Chinese Academy of Sciences for providing SRTM3 DEM, and Weather Underground for the historic precipitation data support. The authors also thank Professor Hong jian You and two anonymous reviewers for their helpful suggestions.

REFERENCES

Berardino P, Fornaro G, Lanari R and Sansosti E. 2002. A new algorithm for surface deformation monitoring based on small baseline differential SAR interferograms. IEEE Transactions on Geoscience and Remote Sensing, 40(11): 2375 – 2383 [DOI: 10.1109/TGRS.2002.803792]

Chen X H and Zhou S F. 1999. Standardized seawall project on Qiantang River. Advances in Science and Technology of Water Resources, 19(4): 39 – 46

Di Martire D, Iglesias R, Monells D, Centolanza G, Sica S, Ramondini M, Pagano L, Mallorquí J J and Calcaterra D. 2014. Comparison between differential SAR interferometry and ground measurements data in the displacement monitoring of the earth-dam of Conzadella Campania (Italy). Remote Sensing of Environment, 148: 58 – 69 [DOI: 10.1016/j.rse.2014.03.014]

Dixon T H, Amelung F, Ferretti A, Novali F, Rocca F, Dokka R, Sella G, Kim SW, Wdowinski S and Whitman D. 2006. Space geodesy: subsidence and flooding in New Orleans. Nature, 441(7093): 587 – 588 [DOI: 10.1038/441587a]

Fan J H, Guo H D, Guo X F, Liu G, Ge D Q and Liu S W. 2008. Monitoring subsidence in tianjin area using interferogram stacking based on coherent targets. Journal of Remote Sensing, 12(1): 111 – 118 [DOI: 10.11834/jrs.20080115]

Ferretti A, Prati C and Rocca F. 2001. Permanent scatterers in SAR interferometry. IEEE Transactions on Geoscience and Remote Sensing, 39(1): 8 – 20 [DOI: 10.1109/36.898661]

Gernhardt S and Bamler R. 2012. Deformation monitoring of single buildings using meter-resolution SAR data in PSI. ISPRS Journal of Photogrammetry and Remote Sensing, 73: 68 – 79 [DOI: 10.1016/j.isprsjprs.2012.06.009]

Hooper A. 2008. A multi-temporal InSAR method incorporating both persistent scatterer and small baseline approaches. Geophysical Research Letters, 35(16): L16302 [DOI: 10.1029/2008GL034654]

Hooper A J. 2006. Persistent scatter radar interferometry for crustal deformation studies and modeling of volcanic deformation. Stanford: Stanford University: 35 – 36

Jiang M, Bian X C, Wu J G, Huang J W, Chen Y M and Chen R P. 2010. Field measurement and numerical simulation of estuarine deposit settlements under embankment loads. Chinese Journal of Rock Mechanics and Engineering, 29(5): 1060 – 1067

Jiang W and Tao C H. 2002. The seawall in Qiantangestuary // Engineered Coasts. Netherlands: Springer, 6: 139 - 150 [DOI: 10.1007/978 - 94 - 017 - 0099 - 3_7]

Ministry of Water Resources of China. 2009. Guide to the implement of Code for design of sea dike project (SL 435 - 2008). Beijing: China WaterPower Press: 198 - 200

Pei Y Y, Liao M S and Wang H M. 2013. Monitoring levee deformation with repeat-track space-borne SAR images. Geomatics and Information Science of Wuhan University, 38(3): 266 - 269

Perissin D and Wang T. 2011. Time-series insar applications over urban areas in china. IEEE Journal of Selected Topics in Applied Earth Observations and Remote Sensing, 4(1): 92 - 100 [DOI: 10.1109/JSTARS.2010.2046883]

Perissin D, Wang Z Y and Lin H. 2012. Shanghai subway tunnels and highways monitoring through Cosmo-SkyMed Persistent Scatterers. ISPRS Journal of Photogrammetry and Remote Sensing, 73: 58 - 67 [DOI: 10.1016/j.isprsjprs.2012.07.002]

Rosen P A, Hensley S, Joughin I R, Li F K, Madsen S N, Rodriguez E and Goldstein R M. 2000. Synthetic aperture radar interferometry. Proceedings of the IEEE, 88(3): 333 - 382 [DOI: 10.1109/5.838084]

Shi X G, Liao M S, Wang T, Zhang L, Shan W and Wang C J. 2014. Expressway deformation mapping using high-resolution TerraSAR-X images. Remote Sensing Letters, 5(2): 194 - 203 [DOI: 10.1080/2150704X.2014.891774]

Xiaoshan District Agricultural and Water Conservancy Bureau. 2009. Typhoon and Surge Defense Plan of Qiantang River Seawall in Xiaoshan, Hangzhou ([2014-05-03]. http://xxgk.xiaoshan.gov.cn/yjgl/yjya/201012/t20101201_225439.htm)

Xu W Q. 2010. District Supervision Bureau monitored the effectiveness of implementation of Standardized Seawall Phase One Project in Outside Section Six to Eight, Xiaoshan inning. Xiaoshan District Agricultural Mechanization and Water Convervancy Bureau. [2014-05-03]. http://www.xsnsw.com/viewnews.asp? id = 3663

Xu Y, He X F, Yang G, Hu P, Dai Q H and Ding X L. 2004. A GPS-based deformation monitoring system for pudong sea-wall. Geotechnical Investigation and Surveying, (1): 43 - 50

Yue D L. 2009. Hidden dange caused by subsidence of seawall in coastal area of Zhejiang Province gradually revealed. Xinhua ([2014-06-13]. http://news.xinhuanet.com/politics/2009-11/26/content_12543902.htm)

Yue J P and Fang L. 2012. Monitoring and Controlling Theory and Techniques for Urban Land Subsidence. Beijing: Science Press: 37 - 50

Zhang W. 2008. Crustal Deformation Monitoring Based on D-InSAR Technology in Hangzhou Area and Study on Deformation Mechanism. Hangzhou: Zhejiang University: 52 - 66

基于时间序列雷达干涉测量的钱塘江海塘形变分析

张云俊[1,3]，万紫[2]，谢酬[1]，邵芸[1]，袁名欢[1,3]，陈武[2]，王新[2]

1. 中国科学院遥感与数字地球研究所，北京 100101；
2. 浙江省水利河口研究院，浙江 杭州 310020；
3. 中国科学院大学，北京 100049

摘　要：形变监测是海塘安全运行的重要组成部分。本文利用杭州地区 2006 年—2010 年获取的 31 景 Envisat-ASAR 影像，根据 MTInSAR（Multi-Temporal InSAR）方法，综合提取 PS（Persistent Scatterer）和 DS（Distributed Scatterer）点，得到密集的钱塘江海塘形变的 InSAR 测量结果。与 28 个点的水准数据对比表明，两者的平均误差为 0.436 mm，最大误差为 5.016 mm，验证了 InSAR 技术毫米级的测量精度和准确性。通过这两种数据的时间序列分析发现，海塘的沉降在空间上具有连续性，其空间分布呈现为单峰下沉曲线；在时间上，则具有明显的线性变化规律，并伴随有短时间范围的小幅度波动。

关键词：MTInSAR，PS，DS，钱塘江海塘，沉降

中图分类号：P228　　**文献标志码**：A

引用格式：张云俊，万紫，谢酬，邵芸，袁名欢，陈武，王新. 2015. 基于时间序列雷达干涉测量的钱塘江海塘形变分析. 遥感学报，19(2)：339－354

Zhang Y J，Wan Z，Xie C，Shao Y，Yuan M H，Chen W and Wang X. 2015. Deformation analysis of the seawall in Qiantang estuary with multi-temporal InSAR. Journal of Remote Sensing，19(2)：339－354 ［DOI：10.11834/jrs.20154055］

1　引　言

钱塘江河口是举世闻名的强潮河口，其南北两岸分布的钱塘江海塘是杭嘉湖平原和萧绍宁平原防御洪水和海潮的重要屏障（Jiang 和 Tao，2002）。由于钱江涌潮破坏力极强，杭州台风、暴雨多发，加之标准海塘大多建在软土地基上，经过多年的运行，因堤身和塘闸的变形引起的安全隐患逐渐显现（岳德亮，2009；陈希海和周素芳，1999）。因此迫切需要开展针对海塘工程的实时安全检测的技术研究。

目前国内的海塘变形监测主要采用传统的水准测量和 GPS 等手段实地观测（岳建平和方露，2012；徐勇等，2004），也有学者利用数值模拟和有限元方法获得模拟结果，通过沉降模型分析海塘与海基软土随时间的沉降规律（姜民 等，2010；水利部，2009）。但这些方法仅针对离散的观测点，无法获得大范围的海塘形变数据；其在空间上仅针对由于工程施工过程造成的周边海塘的变形；在时间上也往往局限于新建海塘的施工期和工程完工后的沉降监测，对海塘的自然沉降过程研究较少。

InSAR（Interferometric Synthetic Aperture Radar）技术可以获取大范围、高精度的地表 3 维和形变信息，具有费用低、广覆盖、全天时全天候和高分辨率的特点（Rosen 等，2000），特别适用于海塘沉降的大范围监测研究；尤其是近几十年来发展起来的以永久散射体 PSInSAR（Permanent ScatterersInSAR）技术（Ferretti 等，2001）和小基线子集 SBAS（Small BAseline Subsets）方法（Berardino 等，2002）为代表的 MTInSAR（Multi-Temporal InSAR）技术，克服了传统 InSAR 技术在空间、时间去相干和大气延迟相位上的影响，使得多基线、长时间序列的 InSAR 地表形

收稿日期：2014-03-17；**修订日期**：2014-06-25；**优先数字出版日期**：2014-07-02

基金项目：水利部公益性行业科研专项经费项目（编号：201201043）

第一作者简介：张云俊（1989—　），男，硕士研究生，现从事 InSAR 理论和应用研究。E-mail：jiuncheung@gmail.com

通信作者简介：万紫（1982—　），男，工程师，现从事水利遥感应用和研究。E-mail：wanzi021@163.com

变监测成为可能。国内外不少学者陆续开展了用于城市地表沉降的 InSAR 应用研究(Dixon 等,2006;Gernhardt 和 Bamler,2012;Perissin 和 Wang,2011;张微,2008;范景辉 等,2008);近年来针对线状目标的 InSAR 形变研究成为热点(Di Martire 等,2014;Perissin 等,2012;Shi 等,2014),但具体到海塘形变的研究则相对较少(裴媛媛 等,2013)。

本文利用 MTInSAR 方法,提取 PS(Persistent Scatterer)和 DS(Distributed Scatterer)点,得到密集的相干目标点的时间序列形变数据;然后在水准测量数据的支持下,对钱塘江海塘形变的空间分布和时间变化进行分析。

2 实验区与数据

实验区是一个 82×40 km^2 的矩形区域(29°59′40″N—30°28′49″N,119°55′06″E—120°50′13″E),主体位于浙江省杭州市。该区地处长江三角洲南沿和钱塘江流域下游,钱塘江从西向东流经整个实验区,覆盖临江海塘约 268 km,如图 1 所示。钱塘江海塘历史悠久,现存的古海塘以明清时期为主,其中大部分已退居二线,部分存留的一线海塘也已经过加固成为标准海塘(陈希海和周素芳,1999),故不在本文讨论范围内。

图 1 实验区的地理位置和 SAR 影像的振幅均值图

(左边底图为杭州地区的微软必应航拍像片,白色矩形表示 31 景 ASAR 影像的覆盖范围,白色箭头指示卫星移动方向,橙色矩形表示实验区范围,红色线条为水准线的位置分布;右边为 31 景多视处理后的 SAR 振幅均值图)

本次实验共获取欧洲太空局提供的杭州地区 Envisat ASAR Stripmap I2 模式 SAR 影像 31 景(重访周期 35 d,C 波段,波长为 5.6 cm),时间跨度为 2006 年 1 月至 2010 年 1 月,入射角为 22.8°,上升轨道,极化方式为 VV(垂直极化),空间分辨率为 20 m(其他参数见表 1,覆盖范围如图 1 中白框所示)。同时收集了钱塘江河口南北两岸海塘在 2009 年 8 月至 2012 年 11 月间测量的 12 期共 136 个点的四等水准测量数据(路线如图 1 中红色线条所示)。另外,还收集了 90 m 空间分辨率的 SRTM3 DEM 和 Weather Underground 提供的杭州地区 2006 年—2010 年的历史气象数据。

3 MTInSAR 处理方法

杭州地处亚热带季风区,四季分明,雨量充沛,森林覆盖率高,使得该区地物在 InSAR 处理中受时间去相干和大气延迟相位影响显著。钱塘江延绵数百公里,两岸地理环境多变,使得海塘上的强散射体分布少而不均,常规的 PSInSAR 方法并不适用。SBAS 方法能够充分挖掘短时间基线和空间基线的干涉相位信息,有效提取到散射特性均一的分布式目标,更适合于海塘的 InSAR 形变观测,但其中的多视处理损失图像分辨率。因此本文利用 Hooper(2008)提出 MTInSAR 方法,综合利用 PSInSAR 和 SBAS 的优点,在不损失空间分辨率的情况下,分别提取 PS 和 DS 点,得到密集、均一的测量点分布,其处理流程如图 2 所示。

在其中的 SBAS 处理中,干涉图的选取采用相干性阈值法(阈值为 0.75),其相干性 ρ 通过基于时间基线 T 和垂直空间基线 $B_\perp$ 的相干性预估函数估计(Hooper,2006):

$$\rho = \left(1 - f\left(\frac{B_\perp}{B_\perp^c}\right)\right) \cdot \left(1 - f\left(\frac{T}{T^c}\right)\right) \tag{1}$$

式中,

$$f(x) = \begin{cases} |x|, |x| \leqslant 1 \\ 1, |x| > 1 \end{cases} \tag{2}$$

式中，$B_{\perp}^{c}$ 为垂直空间基线阈值，对于 ASAR 影像，其值为 1106 m；T^{c} 为时间基线阈值，在此设为 1500 天。为保证形变的成功解算，添加了两个干涉图（图 3 箭头所指），使得 SBAS 干涉网络全局连通。另外，2008-05-29 和 2009-08-27 获取的影像由于强降雨的影响，致使其对应的干涉图中出现严重的不规则大气相位，予以剔除（图 3 中橙色菱形点）。最终 SBAS 方法生成干涉图 63 幅，组合情况如图 3 中虚线所示。

表 1　杭州地区 Envisat-ASAR 影像及其参数

序列号	成像日期	轨道	$B_{\perp}$/m	T/d	Diff_f_DC/Hz
1	2006-01-05	20133	1175.1	−1120	11.32
2	2006-02-09	20634	630.9	−1085	5.51
3	2006-03-16	21135	871.1	−1050	1.15
4	2006-04-20	21636	−336.7	−1015	3.08
5	2006-05-25	22137	439.5	−980	−0.43
6	2006-12-21	25143	585.9	−770	−20.36
7	2007-03-01	26145	120.5	−700	1.21
8	2007-05-10	27147	153.3	−630	7.64
9	2007-08-23	28650	432	−525	10.62
10	2007-11-01	29652	260.4	−455	4.59
11	2007-12-06	30153	−126.2	−420	−9.09
12	2008-02-14	31155	−15.5	−350	1.84
13	2008-03-20	31656	355.3	−315	6.85
14	2008-04-24	32157	300.6	−280	5.13
15	2008-05-29	32658	319.5	−245	6.53
16	2008-07-03	33159	−37.8	−210	−2.00
17	2008-08-07	33660	350.8	−175	3.30
18	2008-09-11	34161	−47.6	−140	8.56
19	2008-10-16	34662	165.4	−105	7.04
20	2008-11-20	35163	−179.4	−70	3.05
21	2008-12-25	35664	151.3	−35	6.73
22	2009-01-29	36165	0	0	0.00
23	2009-03-05	36666	209.8	35	5.70
24	2009-04-09	37167	−140.9	70	6.59
25	2009-05-14	37668	118.4	105	8.59
26	2009-06-18	38169	−104.4	140	7.89
27	2009-07-23	38670	285.5	175	−1.73
28	2009-08-27	39171	390.6	210	15.09
29	2009-10-01	39672	−218.2	245	6.58
30	2009-12-10	40674	3.8	315	−2.11
31	2010-01-14	41175	138.8	350	5.57

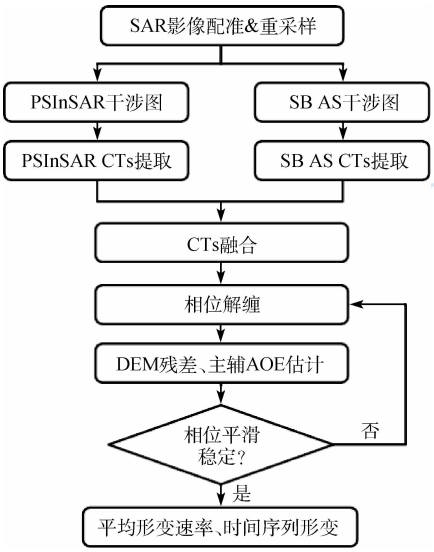

图 2　MTInSAR 处理流程

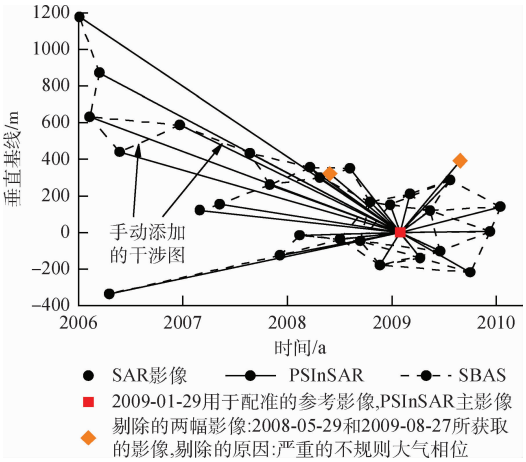

图 3　干涉图组合

4　结果与讨论

4.1　InSAR 结果

根据前面所述方法，由 79 幅干涉图（SBAS 63 幅，PSInSAR 30 幅，重叠 14 幅）计算得到杭州地区 2006 年 1 月至 2010 年 1 月间的地表形变的 InSAR 测量结果，其在雷达视线方向 LOS（Line-Of-Sight）的平均形变速率如图 4 所示。其中，负值表示地物与卫星的距离增加，即沉降；正值则表示抬升。实验区地表在 LOS 方向上的平均形变速率变化范围为 −27.7—11.4 mm/a，对应的反演精度中误差在 0.9—11.4 mm/a；其中，包括杭州市市区在内的大部分地区形变速率中误差在 1.5 mm/a 左右，说明反演结果稳定。

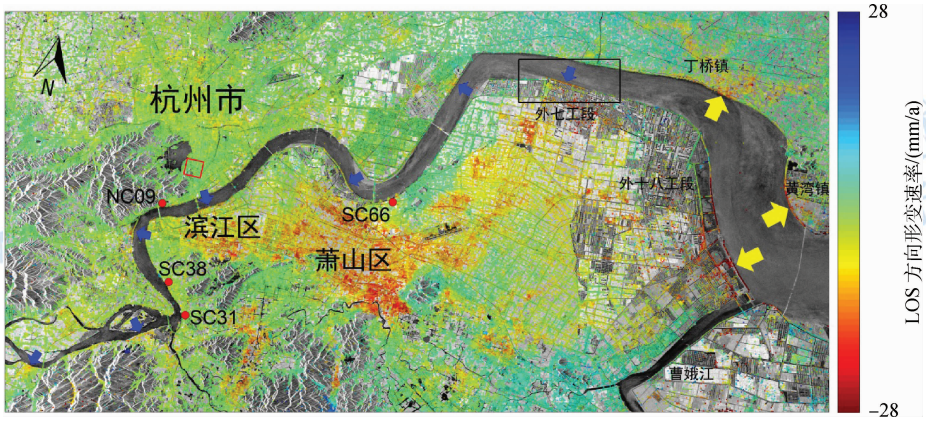

图 4 杭州地区 2006 年 1 月—2010 年 1 月的 LOS 方向形变速率分布
(底图为 31 景 SAR 影像多视处理后的振幅均值图。黄色箭头标记杭州湾海塘的沉降堤段;蓝色箭头标记钱塘江河口海塘的沉降堤段。红色方框为形变结果的参考区域。)

将 PSInSAR 和 MTInSAR 方法在萧山区围垦外五至外九工段海塘(如图 4 中黑色矩形框)的结果进行对比,如图 5 所示。可以明显看出 MTInSAR 方法在海塘上能够提取到更加密集的相干目标点。进一步统计可知:在长约 9 km 的海塘上,PSInSAR 方法提取到 PS 点 36 个,平均点密度为 4/km,与水准测量每 300—500 m 一个测量点的密度(2—3.3/km)相当;而 MTInSAR 方法提取相干目标点 99 个,平均点密度达 11/km,远远超过前两者的测量点密度,证明了 MTInSAR 方法在海塘形变监测上的优势。

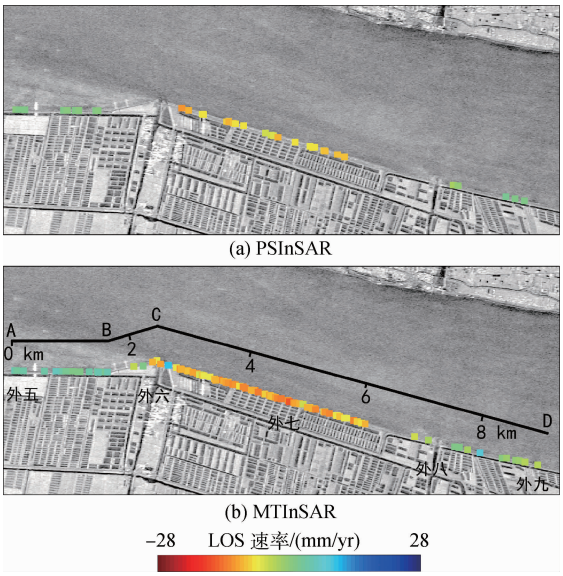

图 5 萧山区围垦外五至外九工段海塘的 InSAR 结果对比

由整个实验区的统计结果可知:钱塘江南北两岸海塘在 4 年间具有明显沉降的堤段有 10 处:7 处位于钱塘江河口(图 4 蓝色箭头标记),3 处位于杭州湾(图 4 黄色箭头标记);且杭州湾海塘的沉降在幅度和范围上均大于钱塘江河口海塘。其中,以杭州湾南岸的外十八工段至曹娥江大闸海塘、北岸的黄湾镇和丁桥镇海塘,以及钱塘江河口南岸的外六至外八工段海塘在沉降幅度和范围上最为显著,其 LOS 方向年均沉降速率均超过 20 mm/a。

4.2 水准数据验证

根据钱塘江河口南北两岸海塘 2009 年—2012 年期间 12 期 136 个点的四等水准测量数据,对 InSAR 结果进行精度验证。为尽可能减小由于水准数据与 InSAR 数据在空间位置和时间上的差异带来的误差,验证数据的选择基于以下 3 个原则:(1)仅选取水准点周围一定空间范围内的相干目标点,考虑到 ASAR 影像 30 m 的空间分辨率,距离阈值设为 100 m;(2)由于海塘结构复杂,不同部分,如堆石、护坡、防浪墙和道路,之间的形变模式并不相同,因此仅选取位于防浪墙及其内侧(水准点的分布位置)的相干目标点;(3)由于两种数据的时间范围并不完全重叠(SAR:2006-01-05—2010-01-14;水准:2009-08-15—2012-12-18),因此仅选取重叠时期的测量数据。最后,将所有符合要求的相干目标点的形变测量值(从 LOS 方向转换到竖直方向)的算术平均值与其相应的水准测量值进行对比。

根据上述条件,选出符合要求的水准点 28 个,其中水准数据的时间范围为 2009-08-15—2009-11-27,InSAR 数据的时间范围为 2009-07-23—2009-12-10,对比结果如图 6 所示。可以看出:两种方法测量的海塘形变趋势大体相近。对比数据统计显示:两

者测量结果的平均误差为 0.436 mm，中误差为 1.582。说明 InSAR 的测量结果与实地水准测量结果吻合较好，能够满足海塘沉降的监测需求。其中，两者结果的最大差值为 5.016 mm，位于 SC68 号点，该水准点对应的相干目标点位于海塘防浪墙内侧道路的井盖上，因此其形变模式显然异于防浪墙或其内侧的连接道路。

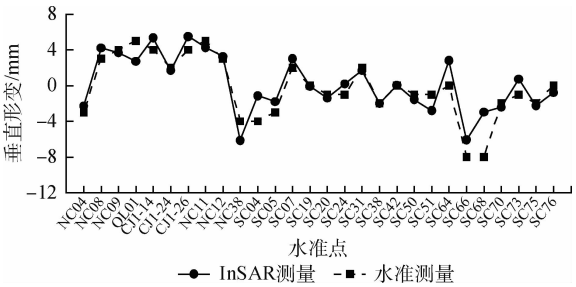

图 6 水准测量与 InSAR 测量的形变量对比

4.3 空间分布

选取萧山区围垦外五至外九工段海塘为研究对象（位置如图 4 中黑色矩形框所示，详图见图 5），对其沉降的空间分布进行分析。该段海塘属萧山围垦北线；其中的外六至外八工段海塘是在 1978 年围堤的基础上，于 2002 年对内凹段进行裁弯取直后建成，以 50 年一遇防洪标准设计；但其护脚不够深，易受冲掏空，当主槽摆动临堤或涌潮顶冲时，抛石护坡的石方冲失严重（萧山区农机水利局，2009）；因此于 2009-12—2010-11 期间，通过杭州市强塘工程，完成了标准塘一期工程施工，按百年一遇防洪标准进行了加固（徐卫桥，2010）。

外五至外九工段海塘可由 3 条线段 AB、BC、CD 近似表示，见图 5（b）；以 A 为起点，将所有相干目标点沿这 3 条线段进行距离换算，得到该段海塘的时间序列的形变空间分布，如图 7 所示。由图 7 可

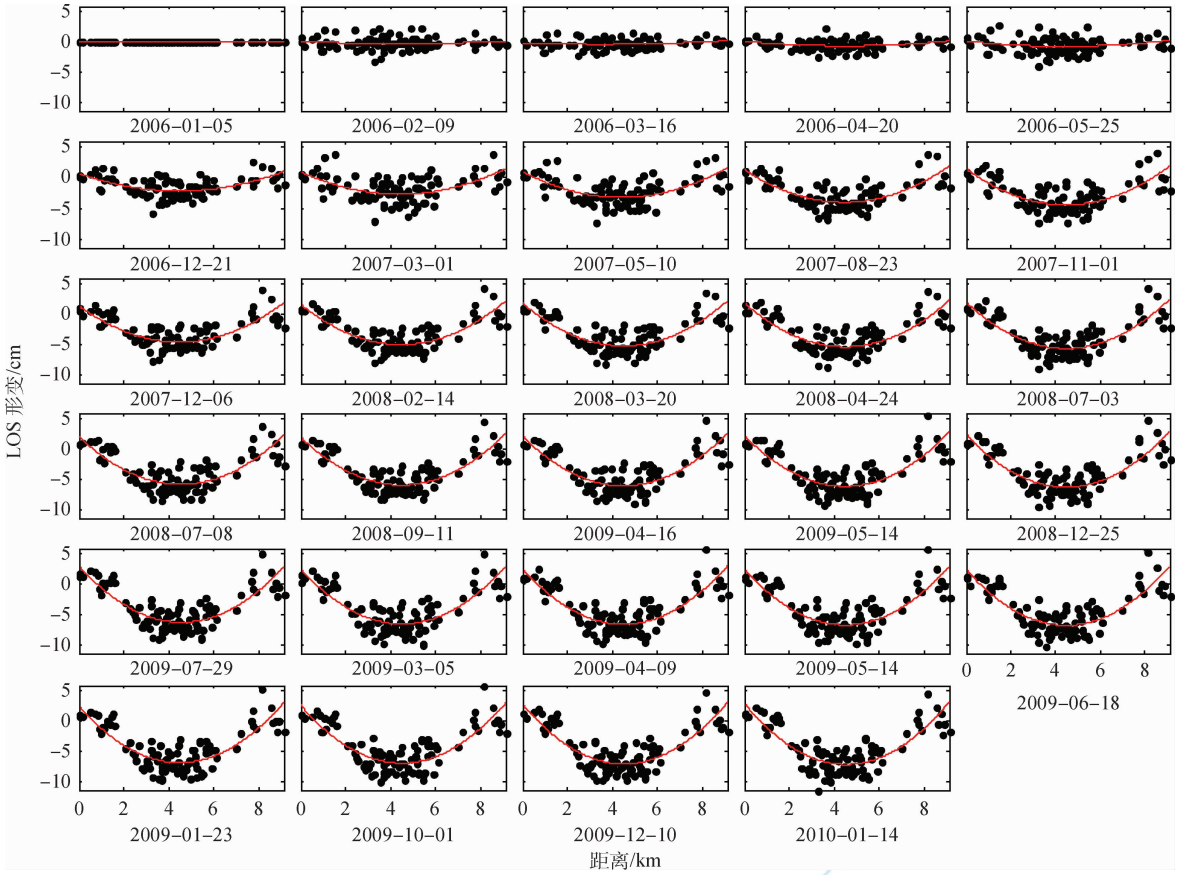

图 7 外五至外九工段海塘形变的时间序列空间分布

（外五至外九工段海塘的位置在图 4 中用黑色矩形框标出，形状可由 3 条线段 AB、BC、CD 近似表示，如图 5(b)所示。所有的形变值均以 2006-01-05 为参考；所有点的距离均以 A 为起点，并沿着 3 条线段进行换算。拟合的形变趋势用红色线条标出。）

知:该段海塘的沉降在空间上连续,其分布满足中间低两边高的单峰下沉曲线。其中:外六至外八工段沉降明显,与其东西两端连接的外五和外九工段则相对稳定。根据时间可知:InSAR 测量的沉降趋势与实际情况吻合。整个实验区地表在 LOS 方向的沉降量的时间序列空间分布如图 8 所示。

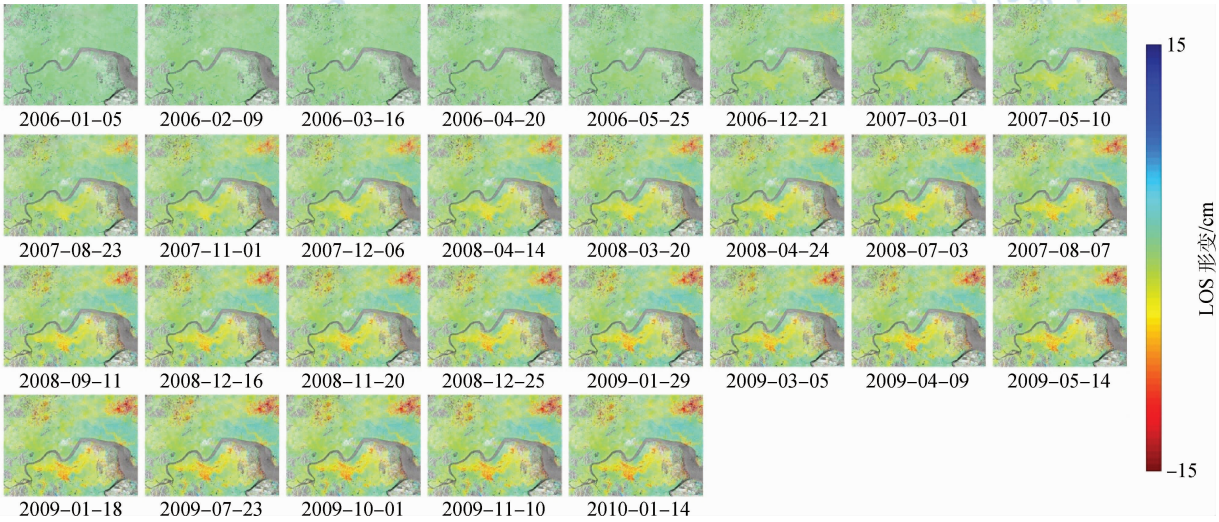

图 8 实验区地表形变的时间序列变化

4.4 时间变化规律

利用 SAR 数据和水准数据重叠时间短、覆盖时间长的特点,对选取的 28 个验证点在长达近 7 年(2006-01—2012-12)的形变随时间的变化规律进行分析。首先,根据水准测量的总形变量,对 28 个点进行分类,结果如图 9。由图 9 可知:它们明显分成 4 种类型。从每种类型中,分别选取一个代表性的点(图 9 中红色标记),进行时间序列分析。4 点的位置在图 4 中用红色圆点标出,分别为:位于上城区钱塘江大桥东北侧的 NC09,位于萧山区闻堰镇南部的 SC31 和北部的 SC38,以及位于萧山区下沙大桥东南侧的 SC66。

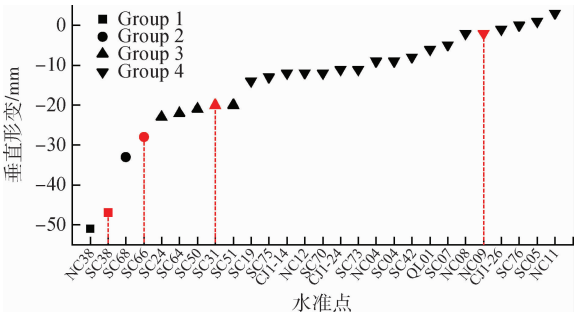

图 9 水准测量总形变量的 28 个点的分类结果

结合 InSAR 和水准测量数据,将 4 个点的沉降量随时间变化关系展示如图 10;图 10 中每个子图中,左半部分的圆点实线表示 InSAR 测量结果,右半部分的方点虚线表示水准测量结果。由图 10 可知:4 个点的沉降量在短时间范围内均有一定的波动,但在长时间范围内则呈现出明显的线性变化规律;其沉降速率按照 NC09、SC31、SC66、SC38 的顺序依次增大。

根据 4 个点的线性形变趋势,对其沉降的时序变化进行线性回归分析,拟合出沉降量随时间的线性变化关系,结果如图 10 中红色实线所示。可以看出:线性拟合结果与 InSAR 和水准测量结果吻合很好,说明两种方法独立测量所得的时间序列沉降趋势一致,进一步验证了 InSAR 测量结果的准确性。根据拟合参数,得到 4 个点的平均沉降速率的估计值,如表 2 所示。沉降量最大的 SC38 平均沉降速率为 12.6 mm/a,其 7 年间的累计沉降量达 8.7 cm;而沉降量最小的 NC09 的平均沉降速率为0.05 mm/a。由图 9 可知,在 28 个点中,沉降最大的 Group1 类仅有 2 个点;而剩下的 26 个点沉降速率均小于 10 mm/a,占了绝大多数,说明钱塘江河口两岸海塘整体上较为稳定。

表 2 2006 年—2012 年 4 个点沉降速率的线性回归估计值

水准点号	SC38	SC66	SC31	NC09
形变速率/(mm/a)	-12.6	-9.1	-4.8	-0.05

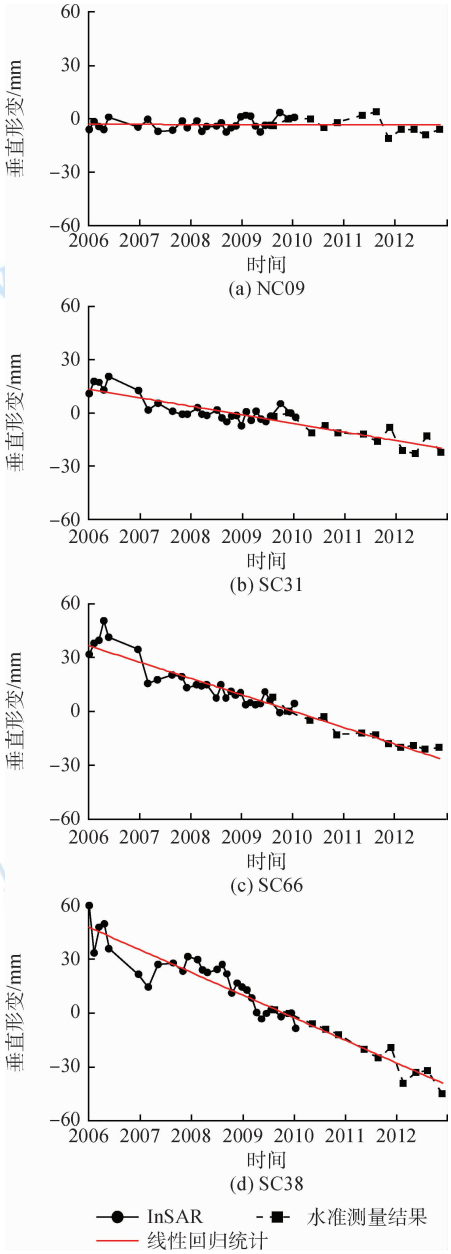

图 10 4 个点在近 7 年间的时间序列沉降

5 结 论

本文利用 MTInSAR 方法，综合提取 PS 点和 DS 点，得到杭州地区 2006-01—2010-01 的地表形变平均速率分布和沉降量的时间序列分布。与实地水准测量数据的对比，验证了 InSAR 测量结果的可靠性和准确性，说明该技术能够满足海塘沉降监测的精度要求。与 PSInSAR 方法对比说明了该方法能够提高了 InSAR 提取的相干目标点数量，使其在海塘上的测量密度上远远超过水准测量方法。共发现了 10 处沉降海塘堤段；且杭州湾海塘沉降段在沉降范围和幅度上均大于钱塘江河口海塘。通过对部分典型的沉降点和堤段的时间序列分析发现，钱塘江海塘的沉降在空间上具有连续性，其空间分布呈现为单峰下沉曲线；在时间上具有明显的线性变化规律，并伴随短时间范围内的小幅度波动；不同的堤段，其沉降速率有所不同，且大部分为轻度沉降。

未来将设计新的处理算法以进一步提高海塘上相干点的分布密度，并深度挖掘海塘沉降的规律及其与所处地质和环境的关系。

志 谢 杭州地区 Envisat ASAR 数据由欧洲航空局提供，DEM 数据由中国科学院计算机网络信息中心地理空间数据云（http://www.gscloud.cn）提供，尤红建研究员对本文提供了有益建议，在此表示衷心的感谢！

参考文献(References)

Berardino P, Fornaro G, Lanari R and Sansosti E. 2002. A new algorithm for surface deformation monitoring based on small baseline differential SAR interferograms. IEEE Transactions on Geoscience and Remote Sensing, 40(11): 2375 – 2383 [DOI: 10.1109/TGRS.2002.803792]

陈希海，周素芳. 1999. 钱塘江海塘标准塘工程. 水利水电科技进展, 19(4): 39 – 46

Di Martire D, Iglesias R, Monells D, Centolanza G, Sica S, Ramondini M, Pagano L, Mallorquí J J and Calcaterra D. 2014. Comparison between differential SAR interferometry and ground measurements data in the displacement monitoring of the earth-dam of Conzadella Campania (Italy). Remote Sensing of Environment, 148: 58 – 69 [DOI: 10.1016/j.rse.2014.03.014]

Dixon T H, Amelung F, Ferretti A, Novali F, Rocca F, Dokka R, Sella G, Kim SW, Wdowinski S and Whitman D. 2006. Space geodesy: subsidence and flooding in New Orleans. Nature, 441(7093): 587 – 588 [DOI: 10.1038/441587a]

范景辉，郭华东，郭小方，刘广，葛大庆，刘圣伟. 2008. 基于相干目标的干涉图叠加方法监测天津地区地面沉降. 遥感学报, 12(1): 111 – 118 [DOI: 10.11834/jrs.20080115]

Ferretti A, Prati C and Rocca F. 2001. Permanent scatterers in SAR interferometry. IEEE Transactions on Geoscience and Remote Sensing, 39(1): 8 – 20 [DOI: 10.1109/36.898661]

Gernhardt S and Bamler R. 2012. Deformation monitoring of single buildings using meter-resolution SAR data in PSI. ISPRS Journal of Photogrammetry and Remote Sensing, 73: 68 – 79 [DOI: 10.1016/j.isprsjprs.2012.06.009]

Hooper A. 2008. A multi-temporal InSAR method incorporating both persistent scatterer and small baseline approaches. Geophysical Research Letters, 35(16): L16302 [DOI: 10.1029/2008GL034654]

Hooper A J. 2006. Persistent scatter radar interferometry for crustal deformation studies and modeling of volcanic deformation. Stanford: Stanford University: 35 – 36

姜民, 边学成, 吴建国, 黄建武, 陈云敏,陈仁朋. 2010. 海堤荷载下海积软土沉降的现场测试和数值模拟. 岩石力学与工程学报, 29(5): 1060 – 1067

Jiang W and Tao C H. 2002. The seawall in Qiantangestuary // Engineered Coasts. Netherlands: Springer, 6: 139 – 150 [DOI: 10.1007/978 – 94 – 017 – 0099 – 3_7]

水利部. 2009. 海堤工程设计规范(SL 435 – 2008)实施指南. 北京: 中国水利水电出版社: 198 – 200

裴媛媛, 廖明生,王寒梅. 2013. 时间序列 SAR 影像监测堤坝形变研究. 武汉大学学报·信息科学版, 38(3): 266 – 269

Perissin D and Wang T. 2011. Time-series insar applications over urban areas in china. IEEE Journal of Selected Topics in Applied Earth Observations and Remote Sensing, 4(1): 92 – 100 [DOI: 10.1109/JSTARS.2010.2046883]

Perissin D, Wang Z Y and Lin H. 2012. Shanghai subway tunnels and highways monitoring through Cosmo-SkyMed Persistent Scatterers. ISPRS Journal of Photogrammetry and Remote Sensing, 73: 58 – 67 [DOI: 10.1016/j.isprsjprs.2012.07.002]

Rosen P A, Hensley S, Joughin I R, Li F K, Madsen S N, Rodriguez E and Goldstein R M. 2000. Synthetic aperture radar interferometry. Proceedings of the IEEE, 88(3): 333 – 382 [DOI: 10.1109/5.838084]

Shi X G, Liao M S, Wang T, Zhang L, Shan W and Wang C J. 2014. Expressway deformation mapping using high-resolution TerraSAR-X images. Remote Sensing Letters, 5(2): 194 – 203 [DOI: 10.1080/2150704X.2014.891774]

萧山区农机水利局. 2009. 杭州市萧山区钱塘江堤塘防御台风暴潮预案. 杭州市萧山区政府. ([2014-05-03]. http://xxgk.xiaoshan.gov.cn/yjgl/yjya/201012/t20101201_225439.htm

徐卫桥. 2010. 区监察局对萧围外六至外八工段标准塘一期工程实施效能监察. 杭州市萧山区农机水利局. [2014-05-03]. http://www.xsnsw.com/viewnews.asp? id = 3663

徐勇, 何秀凤, 杨光, 胡鹏, 戴强华,丁晓利. 2004. 浦东海塘 GPS 位移监测系统. 工程勘测, (1): 43 – 50

岳德亮. 2009. 浙江沿海海塘沉降变形隐患渐显. 新华网 ([2014-04-30]. http://news.xinhuanet.com/politics/2009-11/26/content_12543902.htm)

岳建平,方露. 2012. 城市地面沉降监控理论与技术. 北京: 科学出版社: 37 – 50

张微. 2008. 基于 D-InSAR 的杭州地区地壳形变监测及机理研究. 杭州: 浙江大学: 52 – 66